Asian Journal of Chemistry; Vol. 38, No. 2 (2026), 394-402
ASIAN JOURNAL OF CHEMISTRY
https://doi.org/10.14233/ajchem.2026.35010

Evaluation of Antioxidant Activities of Novel Tetralone-Derived Triazoles Derivatives: Synthesis and *in silico* Studies

PUSHPALATHA VODGALAYYA[1], A.D. SATHISHA[2], B.B. PRABHUDEVA[1], H.R. SHASHANK GOWDA[2], S. NYDILE[2], K.M. ANIL KUMAR[3] and Y.B. BASAVARAJU[1,*]

[1]Department of Studies in Chemistry, Manasagangotri, University of Mysore, Mysuru-570006, India
[2]Division of Biochemistry, School of Life Science, JSS Academy of Higher Education and Research, Shivarathreeshwara Nagara, Mysuru-570015, India
[3]Department of Environmental Science, JSS Academy of Higher Education & Research, Mysuru-570015, India

*Corresponding author: E-mail: ybb2706@gmail.com

Received: 30 September 2025 *Accepted*: 28 December 2025 *Published online*: 31 January 2026 AJC-22256

In present study, twelve novel tetralone-linked triazole derivatives (**6a-l**) were synthesised and structurally characterised using ^{1}H NMR, ^{13}C NMR and mass spectrometric techniques. The antioxidant potential of the synthesised compounds was evaluated through 2,2-diphenyl-1-picrylhydrazyl (DPPH) radical scavenging and lipid peroxidation (LPO) inhibition assays. Among the tested derivatives, compounds **6e**, **6h**, **6d** and **6i** consistently exhibited the strongest antioxidant activities. In the DPPH assay, compound **6e** demonstrated the highest radical-scavenging capacity with 79.9% inhibition at 120 µM, followed by **6h** (64.3%), **6d** (56.18%) and **6i** (51.8%), reflecting a clear dose-dependent response. These findings were further supported by the LPO assay, where the same four derivatives showed significant protection against oxidative damage to lipid membranes. At 120 µM, compound **6e** displayed the most potent activity with showing 79.9% inhibition, while **6h**, **6d** and **6i** exhibited 64.3%, 60.1% and 52.12% inhibition, respectively. The corresponding IC_{50} values (24-30 µM) further confirmed their strong ability to suppress the chain-propagation phase of lipid peroxidation. Moreover, the molecular docking studies were performed to investigate the interactions of the synthesised derivatives with the oxidoreductase protein (PDB ID: 3NM8) and their pharmacokinetic profiles were predicted using *in silico* absorption, distribution, metabolism, excretion and toxicity (ADMET) analysis.

Keywords: Tetralone-linked triazole derivatives, Antioxidant activity, Molecular docking, ADMET analysis.

INTRODUCTION

Free radicals are extremely reactive and unstable chemical entities that provoke oxidative stress in cells [1]. Oxidative stress (OS) results from the overproduction and buildup of reactive oxygen species (ROS) and reactive nitrogen species (RNS), which disrupt the cellular redox equilibrium, hence impairing cellular and tissue function. Elevated levels of free radicals can harm essential biomolecules, including lipids, proteins, enzymes and nucleic acids, leading to the cellular and tissue malfunction [2]. This form of oxidative damage has been associated with the development of various pathological conditions, including cancer, diabetes, cardiovascular diseases, autoimmune disorders, aging, atherosclerosis, myocardial infarction, stroke and neurodegenerative diseases [3]. Consequently, the discovery of effective agents capable of counteracting oxidative stress has become an important focus of current research. Antioxidants play a crucial role in this context by scavenging or neutralising reactive free radicals, thereby limiting oxidative damage to essential biological components [4]. In response to this need, considerable research efforts have been directed toward the design and development of new antioxidant molecules aimed at preventing or alleviating free radical-induced cellular injury [5-7].

In this context, heterocyclic compounds exhibit a wide range of biological activities [8-12]. Among these, triazoles and their derivatives represent a pharmaceutically and medicinally important class of compounds that are widely utilised as antioxidants [13-15], anti-inflammatory agents [16,17], antimicrobial agents [18,19], anticancer agents [20-25] and analgesics [26], among others. In addition, triazoles serve as valuable intermediates in enzymatic reactions for the prepa-

ration of carbonyl compounds and as protecting groups in the synthetic chemistry. The diverse biological and chemical activities of these compounds are attributed to their structural versatility and unique physico-chemical properties. Structural modification of triazole derivatives with different functional groups is believed to enhance their biological efficacy by improving interactions with specific molecular targets [27].

Considering the significant structural and biological relevance of both tetralone and triazole scaffolds (Fig. 1), herein we report the synthesis of twelve new tetralone-linked triazole derivatives (**6a-l**) using a copper-catalysed click chemistry approach, followed by their evaluation for antioxidant and lipid peroxidation inhibitory activity [28]. Although the oxime-triazole motifs and chromanone-based O-((1-substituted-1*H*-1,2,3-triazol-4-yl)methyl)oximes have been described in the literature [29,30], tetralone-derived O-(triazolyl)methyl oxime hybrids remain unexplored. By systematically varying electron-donating, electron-withdrawing and sterically hindered substituents on the phenyl ring, we also provide the first comprehensive SAR analysis for this scaffold. This combined experimental (DPPH and LPO assays) and computational (molecular docking and correlation) investigation provides a novel antioxidant template with tunable activity.

EXPERIMENTAL

All reagents and chemicals were of analytical reagent (AR) grade and procured from Sigma-Aldrich (India), Merck (India) and SD Fine Chemicals (India). Thin-layer chromatography (TLC) was carried out using Merck TLC Silica gel 60 F_{254} aluminum sheets and the spots were visualised under a UV chamber. ^{1}H NMR and ^{13}C NMR spectra were recorded on an Agilent 400 MHz and 100 MHz NMR spectrometer, respectively, using deuterated chloroform ($CDCl_3$) as the solvent and tetramethylsilane (TMS) as the internal standard; chemical shifts are expressed in δ ppm. Mass spectra were recorded on a Mass Lynx SCN781 spectrophotometer operating in time of flight (TOF) mode. Column chromatography was performed on silica gel (60-120 mesh, Merck) using a mixture of hexane and ethyl acetate in varying ratios as eluents. Melting points were determined using the open capillary method on a standard melting point apparatus and are uncorrected.

Synthesis of (*E*)-3,4-dihydronaphthalen-1(2*H*)-one oxime (1-tetralone oxime): A one-step oximation was performed using α-tetralone (2 g, 13.68 mmol), hydroxylamine hydrochloride (1.9 g, 27.36 mmol) and anhydrous sodium acetate (2.24 g, 27.36 mmol) in methanol (20 mL). The reaction mixture was heated under reflux in a 100 mL round-bottom flask equipped with a reflux condenser and magnetic stirrer for 6 h. Upon completion, the solvent was removed under reduced pressure and the residue was dissolved in ethyl acetate and treated with 2 N NaOH. The organic layer was separated using a separatory funnel, washed sequentially with distilled water and brine and concentrated under reduced pressure to yield 1-tetralone oxime as a brown solid (96% yield). The product was used directly in subsequent reactions without further purification.

Synthesis of (*E*)-3,4-dihydronaphthalen-1(2*H*)-one O-prop-2-yn-1-yl oxime: The O-alkylation of 1-tetralone oxime was carried out by dissolving the oxime (1.5 g, 9.31 mmol) in dry DMF (10 mL), followed by the addition of anhydrous K_2CO_3 (2.5 g, 18.63 mmol) as a base. Propargyl bromide (0.7 mL, 9.31 mmol) was added dropwise at 0-5 ºC and the reaction mixture was stirred under the same conditions for 2 h. Upon completion, the reaction was quenched with ice-cold water and extracted with ethyl acetate. The combined organic layers were dried over anhydrous sodium sulphate and concentrated under reduced pressure to yield the crude O-propargylated derivative, which was used directly in subsequent reactions without further purification.

Synthesis of aryl azide *via* diazotisation and azidation: Aniline (1.0 equiv.) was dissolved in a mixture of conc. HCl and water (2:1, v/v) in a round-bottom flask and stirred at room temperature for 10 min. A precooled aqueous solution of sodium nitrite (1.3 equiv.) was then added slowly and the mixture was stirred for an additional 10 min. Subsequently, an aqueous solution of sodium azide (1.3 equiv.) was added

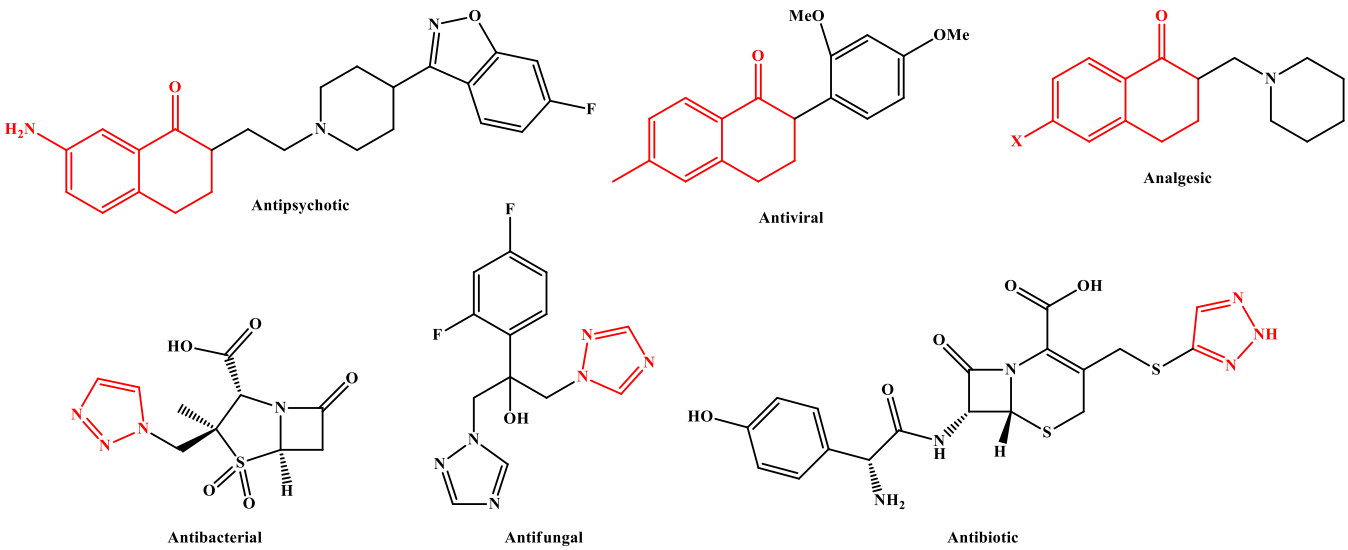

Fig. 1. Tetralone and triazole-containing drugs

dropwise, maintaining the reaction temperature between 0-5 ºC and the reaction mixture was stirred for 2 h. The progress of the reaction was monitored by TLC. Upon completion, water (100 mL) was added and the mixture was extracted with ethyl acetate (5 × 40 mL). The combined organic layers were dried over anhydrous sodium sulphate, filtered and concentrated under reduced pressure to afford the crude aryl azide product.

Synthesis of tetralone-linked triazole derivatives (6a-l): A mixture of (*E*)-3,4-dihydronaphthalen-1(2*H*)-one O-prop-2-yn-1-yl oxime (1.0 equiv.) and aryl azide (1.0 equiv.) was dissolved in dichloromethane (10 mL) in a 100 mL round-bottom flask. Sodium ascorbate (0.6 equiv.) and copper(II) sulfate (0.3 equiv.) were added, followed by water (10 mL). The reaction mixture was stirred vigorously at room temperature for 5 h and the progress was monitored by TLC. Upon completion, water (100 mL) was added and the product was extracted with ethyl acetate (5 × 40 mL). The combined organic layers were dried over anhydrous sodium sulphate, filtered and concentrated under reduced pressure. The crude product was purified by silica gel column chromatography using hexane/ethyl acetate (4:1) as the eluent to afford the pure compounds (**6a-l**) (**Scheme-I**).

(*E*)-3,4-Dihydronaphthalen-1(2*H*)-one O-((1-(4-nitrophenyl)-1*H*-1,2,3-triazol-4-yl)methyl)oxime (6a): Brown semi-solid; yield: 74%; m.p.: 122-124 ºC; ^{1}H NMR (400 MHz, DMSO-d_6, δ ppm): 8.76 (s, 1H, triazole H), 8.21 (dd, *J* = 6.8, 1.2 Hz, 1H, ArH), 7.95-7.81 (m, 4H, ArH), 7.27 (dd, *J* = 7.2, 2.0 Hz, 1H, ArH), 7.22-7.18 (m, 2H, ArH), 5.33 (s, 2H, OCH_2), 2.72-2.50 (m, 4H, CH_2), 1.98-1.73 (m, 2H, CH_2). ^{13}C NMR (101 MHz, DMSO-d_6, δ ppm): 154.8, 144.9, 144.5, 140.1, 134.8, 131.6, 130.2, 129.7, 129.5, 129.1, 128.0, 126.6, 126.2, 125.9, 124.4, 67.1, 29.3, 24.5, 21.4, LCMS (ESI, *m/z*) calcd. for $C_{19}H_{17}N_5O_3$ 363.3770; found (M+H) 364.0365.

(*E*)-3,4-Dihydronaphthalen-1(2*H*)-one O-((1-(4-chlorophenyl)-1*H*-1,2,3-triazol-4-yl)methyl)oxime (6b): White solid; yield: 80%; m.p.: 108-110 ºC; ^{1}H NMR (400 MHz, $CDCl_3$, δ ppm): 8.0 (s, 1H, triazole H), 7.97 (d, *J* = 8.0, 1H ArH), 7.69 (dd, *J* = 6.9, 1.8 Hz, 2H, ArH), 7.49 (dd, *J* = 6.8, 1.8 Hz, 2H, ArH), 7.25 (d, *J* = 6.0 Hz, 2H, ArH), 7.14 (d, *J* = 7.5 Hz, 1H, ArH), 5.41 (s, 2H, OCH_2), 2.79-2.73 (m, 4H, CH_2), 1.87-1.81 (m, 2H, CH_2); ^{13}C NMR (101 MHz, $CDCl_3$, δ ppm): 155.2, 146.3, 139.9, 135.7, 134.6, 130.5, 130.0, 129.3, 128.8, 126.5, 124.3, 121.9, 121.2, 67.5, 29.8, 24.6, 21.4; LCMS (ESI, *m/z*) calcd. for $C_{19}H_{17}ClN_4O$ 352.8220; found (M+H) 353.4561.

(*E*)-3,4-Dihydronaphthalen-1(2*H*)-one O-((1-(4-bromophenyl)-1*H*-1,2,3-triazol-4-yl)methyl)oxime (6c): White solid; yield: 74%; m.p.: 110-112 ºC; ^{1}H NMR (400 MHz, $CDCl_3$, δ ppm): 8.00 (s, 1H. triazole H), 7.97(d, *J* = 1.2 Hz, 1H), 7.64 (d, *J* = 1.1 Hz, 4H, ArH), 7.26 (d, *J* = 1.5 Hz, 1H, ArH), 7.21-7.13 (m, 1H, ArH), 5.41 (s, 2H, OCH_2), 2.79-2.73 (m, 4H, CH_2), 1.87-1.82 (m, 2H, CH_2); ^{13}C NMR (101 MHz, $CDCl_3$, δ ppm): 155.2, 146.3, 139.9, 136.2, 133.0, 130.6, 129.3, 128.8, 126.5, 124.4, 122.5, 122.2, 121.1, 67.6, 29.8, 24.6, 21.5; LCMS (ESI, *m/z*) calcd. for $C_{19}H_{17}BrN_4O$ 396.1091; found (M+H) 397.2345.

(*E*)-3,4-Dihydronaphthalen-1(2*H*)-one O-((1-(2,3-dichlorophenyl)-1*H*-1,2,3-triazol-4-yl)methyl)oxime (6d): White solid; yield: 74%; m.p.: 120-122 ºC; ^{1}H NMR (400 MHz, $CDCl_3$, δ ppm): 8.04 (s, 1H, triazole H), 7.98 (dd, *J* = 7.9, 1.1 Hz, 1H, ArH), 7.63 (dd, *J* = 8.1, 1.5 Hz, 1H, ArH), 7.55 (dd, *J* = 8.1, 1.5 Hz, 1H, ArH), 7.38 (m, 1H, ArH), 7.25 (m, 1H, ArH), 7.19 (m, 1H, ArH), 7.13 (dd, *J* = 7.5, 0.8 Hz, 1H, ArH), 5.44 (s, 2H, OCH_2), 2.79-2.72 (m, 4H, CH_2), 1.87-1.80 (m, 2H, CH_2); ^{13}C NMR (101 MHz, $CDCl_3$, δ ppm): 155.2, 145.2, 139.8, 134.7, 131.6, 129.3, 128.8, 128.0, 127.82, 127.02, 126.4, 126.3, 125.3, 124.3, 67.4, 29.8, 24.6, 21.4; LCMS (ESI, *m/z*) calcd. for $C_{19}H_{16}Cl_2N_4O$ 386.0701; found (M+H) 387.6257.

(*E*)-3,4-Dihydronaphthalen-1(2*H*)-one O-((1-(4-fluorophenyl)-1*H*-1,2,3-triazol-4-yl)methyl)oxime (6e): Brown solid; yield: 81%; m.p.: 118-120 ºC; ^{1}H NMR (400 MHz,

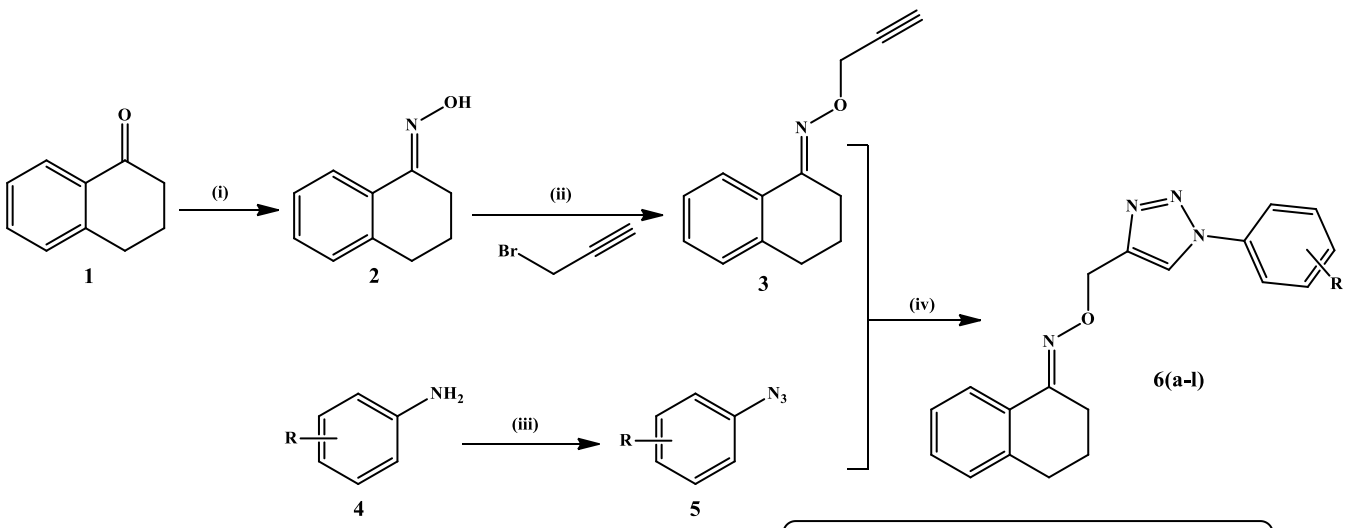

Scheme-I: The synthetic pathway for the synthesis of compounds (**6a-l**)

$CDCl_3$, δ ppm): 8.0 (s, 1H, triazole H), 7.97 (d, *J* = 9.5 Hz, 1H, ArH), 7.70 (d, *J* = 4.8 Hz, 1H), 7.64 (d, *J* = 1.1 Hz, 4H, ArH), 7.25-7.13 (m, 2H, ArH), 5.41 (s, 1H, OCH_2), 2.78-2.72 (m, 4H, CH_2), 1.87-1.80 (m, 2H, CH_2); ^{13}C NMR (101 MHz, $CDCl_3$, δ ppm): 163.7, 155.1, 146.1, 139.8, 133.4, 130.5, 129.3, 128.8, 126.4, 124.3, 122.8, 121.5, 116.9, 116.7, 67.6, 29.8, 24.6, 21.4; LCMS (ESI, *m/z*) calcd. for $C_{19}H_{17}FN_4O$ 336.1386; found (M+H) 337.0877.

(*E*)-3,4-Dihydronaphthalen-1(2*H*)-one O-((1-phenyl-1*H*-1,2,3-triazol-4-yl)methyl)oxime (6f): White solid; yield: 72%; m.p.: 116-118 ºC; ^1H NMR (400 MHz, $CDCl_3$, δ ppm): 8.03 (s, 1H, triazole H), 8.01-7.99 (m, 1H, ArH), 7.75-7.73 (m, 2H, ArH), 7.54-7.50 (m, 2H, ArH), 7.45-7.41 (m, 1H, ArH), 7.24-7.23 (m, 1H, ArH), 7.22-7.18 (m, 1H, ArH), 7.14 (d, *J* = 7.5 Hz, 1H, ArH), 5.42 (s, 2H, OCH_2), 2.79-2.73 (m, 4H, CH_2), 1.87-1.81 (m, 2H, CH_2); ^{13}C NMR (101 MHz, $CDCl_3$, δ ppm): 155.1, 145.9, 139.8, 137.2, 130.6, 129.8, 129.3, 128.9, 128.8, 126.4, 124.3, 121.4, 120.8, 67.6, 29.8, 24.6, 21.4; LCMS (ESI, *m/z*) calcd. for $C_{19}H_{18}N_4O$ 318.1481; found (M+H) 319.4365.

(*E*)-3,4-Dihydronaphthalen-1(2*H*)-one O-((1-(*p*-tolyl)-1*H*-1,2,3-triazol-4-yl)methyl)oxime (6g): White solid; yield: 74%; m.p.: 114-116 ºC; ^1H NMR (400 MHz, $CDCl_3$, δ ppm): 8.23 (s, 1H, triazole H), 7.99 (d, *J* = 8.3 Hz, 2H, ArH), 7.73-7.69 (m, 2H, ArH), 7.24-7.13 (m, 4H, ArH), 5.41 (s, 2H, OCH_2), 2.79-2.73 (m, 4H, CH_2), 2.43 (s, 3H, CH_3), 1.87-1.81 (m, 2H, CH_2); ^{13}C NMR (101 MHz, $CDCl_3$, δ ppm): 163.8, 155.2, 146.2, 139.9, 130.6, 129.3, 128.8, 126.5, 124.3, 122.9, 122.8, 121.6, 117.0, 116.7, 67.6, 31.7, 29.8, 24.6, 21.5; LCMS (ESI, *m/z*) calcd. for $C_{20}H_{20}N_4O$ 332.1637; found (M+H) 333.1589.

(*E*)-1-(4-(4-((((3,4-Dihydronaphthalen-1(2*H*)-ylidene)-amino)oxy)methyl)-1*H*-1,2,3-triazol-1-yl)phenyl)ethan-1-one (6h): Brown gummy mass; yield: 74%; m.p.: 114-116 ºC; ^1H NMR (400 MHz, $CDCl_3$, δ ppm): 8.13 (s, 1H, triazole H), 8.10 (dd, *J* = 6.8, 4.8 Hz, 2H, ArH), 7.99 (dd, *J* = 7.8, 1.1 Hz, 2H, ArH), 7.88 (dd, *J* = 6.9, 2.0 Hz, 1H, ArH), 7.26-7.24 (m, 1H, ArH), 7.21-7.13 (m, 1H, ArH), 7.14 (d, *J* = 7.5 Hz, 1H, ArH), 5.42 (s, 2H, OCH_2), 2.79-2.73 (m, 4H, CH_2), 2.65 (s, 3H, CH_3), 1.85 (m, 2H, CH_2); ^{13}C NMR (101 MHz, $CDCl_3$, δ ppm): 196.8, 155.3, 146.5, 140.2, 139.9, 136.8, 130.5, 130.2, 129.3, 128.8, 126.4, 124.3, 121.1, 120.2, 67.4, 29.8, 26.8, 24.6, 21.4; LCMS (ESI, *m/z*) calcd. for $C_{21}H_{20}N_4O_2$ 360.1586; found (M+H) 361.0579.

(*E*)-3,4-Dihydronaphthalen-1(2*H*)-one O-((1-(2,4-dichlorophenyl)-1*H*-1,2,3-triazol-4-yl)methyl)oxime (6i): White solid; yield: 70%; m.p.: 110-112 ºC; ^1H NMR (400 MHz, $CDCl_3$, δ ppm): 8.08 (s, 1H, triazole H), 8.01 (dd, *J* = 6.2, 1.2 Hz, 1H, ArH), 7.90 (s, 1H, ArH), 7.88 (d, *J* = 7.9 Hz, 1H, ArH), 7.65 (dd, *J* = 12.0, 8.0 Hz, 2H, ArH), 7.26-7.140 (m, 3H, ArH), 5.43 (s, 2H, OCH_2), 2.79-2.72 (m, 4H, CH_2), 1.86-1.82 (m, 2H, CH_2); ^{13}C NMR (101 MHz, $CDCl_3$, δ ppm): 155.3, 145.8, 144.5, 139.9, 133.9, 130.8, 130.4, 130.3, 129.2, 128.7, 128.1, 126.4, 125.6, 124.7, 124.3, 67.4, 29.7, 24.8, 21.3; LCMS (ESI, *m/z*) calcd. for $C_{19}H_{16}Cl_2N_4O$ 386.0701; found (M+H) 387.0621.

(*E*)-3,4-Dihydronaphthalen-1(2*H*)-one O-((1-(3-bromophenyl)-1*H*-1,2,3-triazol-4-yl)methyl)oxime (6j): Brown solid; yield: 75%; m.p.: 114-116 ºC; ^1H NMR (400 MHz, $CDCl_3$, δ ppm): 8.08 (s, 1H, triazole H), 8.06 (dd, *J* = 7.9, 1.1 Hz, 1H, ArH), 7.90 (s, 1H), 7.78 (m, 1H, ArH), 7.68-7.63 (m, 1H, ArH), 7.26-7.140 (m, 3H, ArH), 5.43 (s, 2H, OCH_2), 2.79-2.72 (m, 4H, CH_2), 1.85-1.82 (m, 2H, CH_2); ^{13}C NMR (101 MHz, $CDCl_3$, δ ppm): 155.3, 145.9, 144.5, 139.8, 133.9, 130.9, 130.5, 130.3, 129.3, 128.7, 128.1, 126.4, 125.6, 124.8, 124.4, 77.5, 77.2, 76.8, 67.4, 29.8, 24.6, 21.4; LCMS (ESI, *m/z*) calcd. for $C_{19}H_{17}BrN_4O$ 396.0586; found (M+H) 397.0967.

(*E*)-3,4-dihydronaphthalen-1(2*H*)-one O-((1-(2-chlorophenyl)-1*H*-1,2,3-triazol-4-yl)methyl)oxime (6k): Brown semi-solid; yield: 70%; m.p.: 106-108 ºC; ^1H NMR (400 MHz, $CDCl_3$, δ ppm): 8.06 (s, 1H, triazole H), 7.99 (dd, *J* = 7.8, 1.1 Hz, 1H, ArH), 7.66-7.62 (m, 1H, ArH), 7.59-7.55 (m, 1H, ArH), 7.47-7.43 (m, 2H, ArH), 7.25 (dd, *J* = 7.4, 1.5 Hz, 1H, ArH), 7.23-7.18 (m, 1H, ArH), 7.13 (dd, *J* = 7.5, 0.8 Hz, 1H, ArH), 5.44 (s, 2H, OCH_2), 2.79-2.72 (m, 4H, CH_2), 1.84-1.81 (m, 2H, CH_2); ^{13}C NMR (101 MHz, $CDCl_3$, δ ppm): 155.0, 144.9, 139.7, 135.02, 130.8, 130.7, 130.5, 129.2, 128.7, 128.6, 127.9, 127.8, 126.3, 125.3, 125.3, 124.3, 67.4, 29.8, 24.6, 21.4; LCMS (ESI, *m/z*) calcd. for $C_{19}H_{17}ClN_4O$ 352.1091; found (M+H) 353.2654.

(*E*)-3,4-Dihydronaphthalen-1(2*H*)-one O-((1-(3-nitrophenyl)-1*H*-1,2,3-triazol-4-yl)methyl)oxime (6l): White solid; yield: 84%; m.p.: 124-126 ºC; ^1H NMR (400 MHz, $CDCl_3$, δ ppm): 8.60 (s,1H, triazole H), 8.59 (d, *J* = 8 Hz, 1H, ArH), 8.30 (m, 1H, ArH), 8.19 (d, *J* = 8.1, 1.0 Hz, 1H, ArH), 7.99 (dd, *J* = 7.8, 1.2 Hz, 1H, ArH), 7.75 (m, 1H, ArH), 7.26-7.24 (m, 1H, ArH), 7.21 (d, *J* = 7.6, 1.4 Hz, 1H, ArH), 7.15-7.13 (m, 1H, ArH), 5.43 (s, 2H, OCH_2), 2.80-2.73 (m, 4H, CH_2), 1.86-1.82 (m, 2H, CH_2); ^{13}C NMR (101 MHz, $CDCl_3$, δ ppm): 155.4, 149.0, 146.9, 139.8, 137.9, 131.1, 130.5, 129.4, 128.8, 126.5, 126.2, 124.4, 123.3, 121.2, 115.5, 67.4, 29.8, 24.6, 21.5; LCMS (ESI, *m/z*) calcd. for $C_{19}H_{17}N_5O_3$ 363.1331; found (M+H) 364.3657.

Antioxidant activity

DPPH radical scavenging assay: DPPH radical scavenging activity was done using the reported method; the reaction mixture containing 1 mL of DPPH solution (0.1 mmol/L, in 95% ethanol v/v) with different concentrations of the extract was shaken and incubated for 20 min at room temperature and the absorbance was read at 517 nm against a blank. The radical scavenging activity was measured as a decrease in the absorbance of DPPH and calculated using the following equation [31,32]:

$$\text{Effect of scavenging (\%)} = \left(1 - \frac{A_{\text{sample}}(517\text{ nm})}{A_{\text{control}}(517\text{ nm})}\right) \times 100$$

Lipid peroxidation method: Liver excised from adult male Wister rats, was homogenised (20 g/100 mL tris buffer) in 0.02 mol/L tris buffer (pH 7.4). Microsomes were isolated by the calcium aggregation method. A 100 μL of liver microsomal suspension (0.5 mg protein) was incubated with 1 mmol/L each of $FeSO_4$ and ascorbic acid with or without extract in a total volume of 1 mL in 0.1 mol/L phosphate buffer (pH 7.4). After incubation at 37 ºC for 60 min, thiobarbituric acid (TBA) (0.67 g/100 mL water) was added to the reaction mixt-

ure and boiled for 15 min. The thiobarbituric acid reactive substances (TBARS) was calculated from the absorbance at 535 nm, where butylated hydroxyanisole (BHA) was used as the positive control [33].

Measurement of reducing power: The compounds were taken in different concentrations in phosphate buffer (0.2 mol/L, pH 7.4) and incubated with $K_3[Fe(CN)_6]$ (1 g/100 mL water) at 50 ºC for 20 min. the reaction was terminated by adding tricarboxylic acid (TCA) solution (10 g/100 mL water), centrifuged at 3000 rpm for 10 min and the supernatant was mixed with $FeCl_3$ (0.1 g/100 mL water), finally measured the absorbance at 700 nm. The increased absorbance of the reaction mixture indicated increased reducing power.

Molecular docking studies: The molecular docking of the synthesised compounds **6a-le** with oxidoreductase enzyme (PDB ID: 3NM8), which was selected due to its structural relevance and availability of a high-resolution crystal structure suitable for ligand-receptor interaction studies. The ligands were drawn in ChemDraw 16.0, converted to 3D SDF format and energy-minimised using the built-in tools in PyRx. The protein structure was retrieved from the Protein Data Bank and preparation steps included removal of water molecules, heteroatoms and the native ligand, followed by addition of polar hydrogens and assignment of Kollman charges using AutoDock Tools 1.5.7. Docking was performed on the entire receptor surface (blind docking) using AutoDock Vina 1.1.2 integrated in PyRx 0.8, where the grid box was set large enough to cover the complete protein (center: X = -14.509, Y = 2.6305, Z = 8.2480; dimension (Å) $x = 62.2322$, $y = 60.3700$, $z = 82.8575$). The exhaustiveness was set to 8 and for each ligand, multiple poses were generated, with the lowest-energy conformation selected for interpretation. Docking protocol validation was carried out by re-docking the native ligand into the receptor, which produced an RMSD value of < 2.0 Å, confirming the reliability of the setup. A known standard inhibitor (insert positive control name) was also docked under identical conditions for comparative evaluation. The resulting protein-ligand interactions were visualised using BIOVIA Discovery Studio Visualizer 2025 to identify hydrogen bonding, hydrophobic, π-interactions and other non-covalent contacts [34-36].

ADMET studies: The physico-chemical and pharmacokinetic parameters of the synthesised compounds **6a-l** were predicted using the ADMET lab 2.0 web-based platform to assess their drug-likeness, absorption and blood-brain barrier (BBB) permeability [37].

RESULTS AND DISCUSSION

The synthesis of tetralone-linked triazole derivatives **6a-l** was accomplished *via* a multi-step route starting from α-tetralone, which was initially converted to its oxime through reaction with hydroxylamine in the presence of sodium acetate, which provides a mildly basic environment. In this step, the carbonyl group of α-tetralone reacts with hydroxylamine to form a stable oxime (C=NOH) moiety, in excellent yield. Subsequently, O-alkylation of the oxime was carried out by propargylation. Potassium carbonate was employed to generate the reactive oxime anion, which then displaced the bromide from propargyl bromide *via* a straightforward nucleophilic substitution.

On the other hand, a series of aryl azides was synthesised from substituted anilines. The anilines were first converted into diazonium salts using sodium nitrite under acidic conditions, followed by substitution of the diazonium group using sodium azide at low temperature to maintain selectivity. Finally, the propargylated oxime and the aryl azides were coupled in a copper-catalysed "click" reaction. In the presence of sodium ascorbate and copper sulphate, the terminal alkyne and azide underwent smooth cycloaddition at room temperature to form the triazole ring with complete regioselectivity. This strategy proved to be efficient, afforded consistently high yields and allowed access to a diverse set of tetralone-triazole hybrids through a concise sequence of operationally simple steps.

Antioxidant activity

DPPH radical scavenging assay: The DPPH radical scavenging assay of the synthesised compounds **6a-l**. Compounds **6d**, **6e**, **6h** and **6i** showed the strongest and most dose-dependent activity. The compound **6e** was the most effective, showing 79.9% inhibition at 120 μM, whereas compound **6h** was the second most effective, reaching 64.3% inhibition at 120 μM. Compounds **6d** and **6i** also showed moderate activity, 56.18% and 51.8% inhibition, respectively, at 120 μM. Overall, the results indicate that compound **6e** possesses the strongest DPPH radical scavenging potential among the tested series, making it a promising candidate for further antioxidant studies. The results are summarised in Fig. 2.

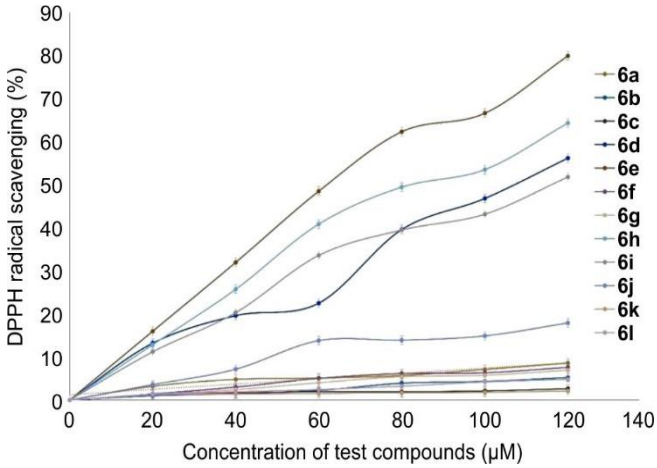

Fig. 2. Antioxidant activity of synthesised compounds (**6a-l**)

Lipid peroxidation method: The lipid peroxidation (LPO) inhibitory activity of compounds **6a-l** was assessed at concentrations of 40, 80 and 120 μM. Of all the derivatives tested, compounds **6d**, **6e**, **6h** and **6i** had the highest amounts of membrane protection. At 120 μM, compound **6e** showed the most potent inhibition (79.9%), followed by **6h** (64.3%), **6d** (60.1%) and **6i** (52.12%). Correspondingly, their IC_{50} values ranged from 24-30 μM, confirming their strong ability to interrupt the chain-propagation phase of lipid peroxidation and validating lipid membrane protection as a key outcome of their radical-scavenging mechanism. In contrast, the remaining compounds demonstrated moderate to negligible activity, with inhibition typically below 15% at 120 μM, suggesting limited potential as LPO inhibitors (Fig. 3). The results show

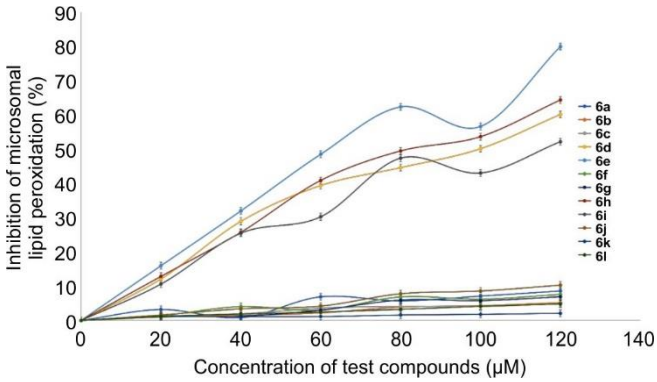

Fig. 3. Lipid peroxidase activity of synthesised compounds (**6a-l**)

that the radical-scavenging ability of the active compound assumed in the initial tests was applicable to the biologically-related LPO model, which mimics the oxidative damage to lipid membranes.

Comparison of IC_{50} values (potency): The antioxidant potential of 12 synthesised compounds **6a-l** was comprehensively evaluated using two distinct *in vitro* mechanistic assays the DPPH radical scavenging assay and the microsomal lipid peroxidation inhibition assay. In comparison, compounds **6d**, **6h** and **6i** show comparable potency in both the DPPH and lipid peroxidation assays, indicating they are effective free-radical scavengers and strong inhibitors of lipid peroxidation, inhibiting membrane damage. Compounds **6a**, **6b**, **6c**, **6f**, **6g**, **6j**, **6k** and **6l** all have very low IC_{50} values in the bar chart, generally below 5 μM. The comparison results are depicted in Fig. 4.

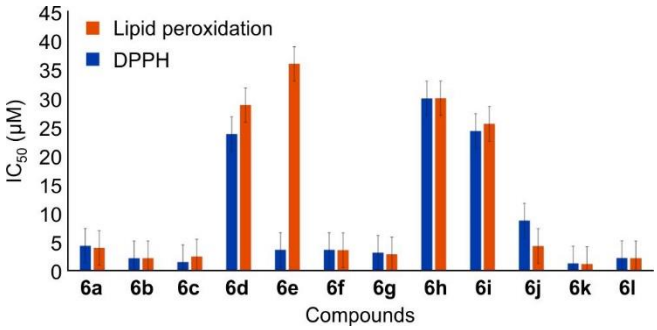

Fig. 4. Comparison of IC_{50} values for DPPH assay and microsomal peroxidation (All the values are represented in mean ± SEM and experiments conducted in triplicate)

Structure-activity relationship (SAR) analysis: A systematic evaluation of the antioxidant properties of compounds **6a-l**, as influenced by their substituents, revealed clear electronic and steric trends governing their DPPH radical-scavenging and lipid peroxidation (LPO) inhibitory activities. The SAR demonstrates that electron-withdrawing substituents on the phenyl ring generally enhance antioxidant potency, as they facilitate a more efficient hydrogen-atom transfer process. Those compounds containing chloro- and acetyl- groups showed significant activity, which can be attributed to the fact that the compounds were able to adjust the bond dissociation energy (BDE) in a favourable fashion, thus being more effective to inhibit both processes of DPPH and LPO. In contrast, compounds with strong electron-withdrawing groups (–NO_2 and –CN) displayed markedly reduced activity (IC_{50} > 120 μM). These groups overreact with BDE, inactivate the aromatic ring and entirely inhibit radical stabilisation, producing insignificant antioxidant activities. Also, the ortho-substituted derivatives were less active because of the steric crowding around the reactive centre. These substituents do not only withdraw electron density, but provide steric hindrance, blocking access of DPPH and lipid peroxyl radicals to the active site, further lowering the efficiency of antioxidants.

Molecular docking studies: Molecular docking was performed to investigate the interactions of the synthesised compounds with the oxidoreductase enzyme (PDB ID: 3NM8), one of the most important proteins in redox control and antioxidant activities and the results are shown in Table-1. The docking pose demonstrated that the ligand enters the active site of the enzyme and it interacts with a number of stabilising forces. The compound formed hydrogen bonds as depicted in the 3D and 2D interactions diagrams, with Ala44 and Gly143, which play an essential role in anchoring the molecule within the catalytic pocket. Furthermore, π-π stacking and π-alkyl interactions were observed with residues Ala40, Ala44 and Lys47, enhancing the overall hydrophobic stabilisation of the complex. The existence of the van der Waals forces with residues including Ile39, Ala40 and Gly143 also contributes to the good accommodation of the compound in the binding groove (Fig. 5). The standard drug was docked so as to give a reference point of comparison and to ensure that the docking protocol was valid. The interaction profile of the 3D interaction showed that the standard ligand had a conventional hydrogen bond with Gly212. Additional carbon-hydrogen bonds with Gly216 stabilised the ligand orientation. Several hydrophobic contacts involving Val211, Val218, Pro201 and Val217 contributed significantly to the overall nonpolar stabilisation characteristic of high-affinity binding modes. Furthermore, π-based interactions, including a π-σ interaction with Trp210 and an amide-π stacked interaction with Pro201, indicate strong aromatic complementarity between the ligand and the receptor environment. The 2D interaction map also highlighted van der Waals interactions with surrounding residues Ala159, His208, Glu158, Arg206, Thr156 and Asn205 (Fig. 6).

TABLE-1
MOLECULAR DOCKING RESULTS OF SYNTHESISED COMPOUNDS (**6a-l**)

Compounds	Docking score (kcal mol^{-1})	Compounds	Docking score (kcal mol^{-1})
6a	-6.8	**6h**	-8.3
6b	-5.9	**6i**	-6.7
6c	-7.6	**6j**	-7.6
6d	-7.7	**6k**	-6.2
6e	-8.1	**6l**	-6.4
6f	-8.0	DPPH	-7.6
6g	-7.4		

All these non-covalent contacts mean the ligand has a fixed shape in the active site, which may limit enzyme oxidative activities. Effective antioxidant chemicals have a balance between hydrogen-bonding and hydrophobic contacts, as observed by the interaction profile. The computational

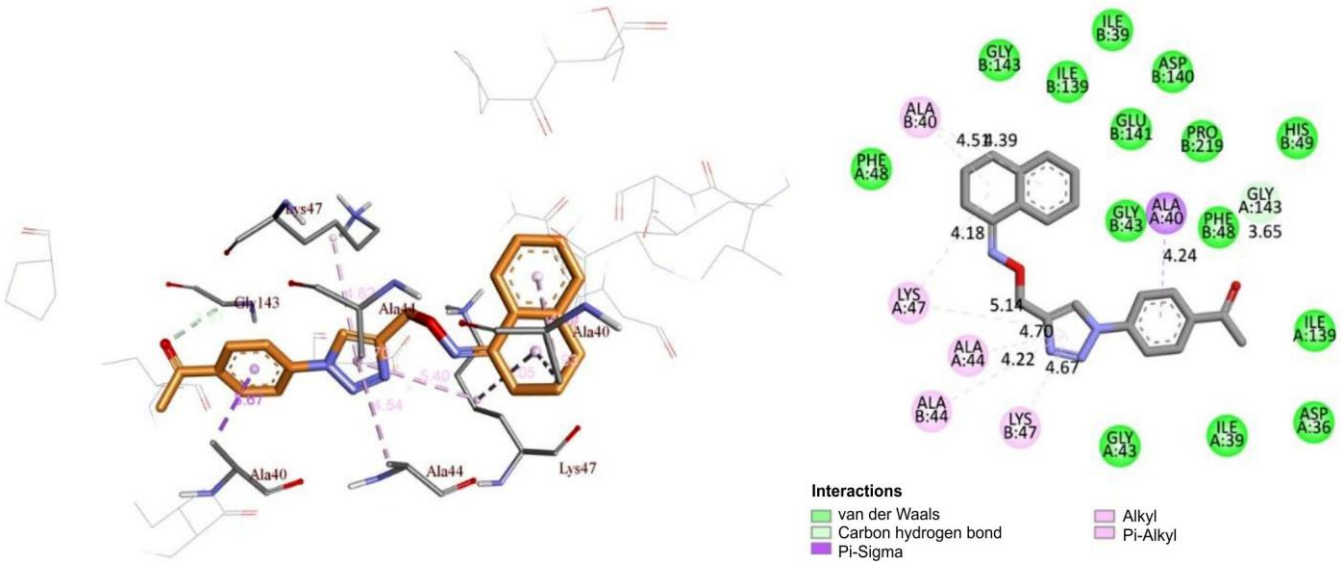

Fig. 5. 3D and 2D molecular docking outcome of lead compound **6h**

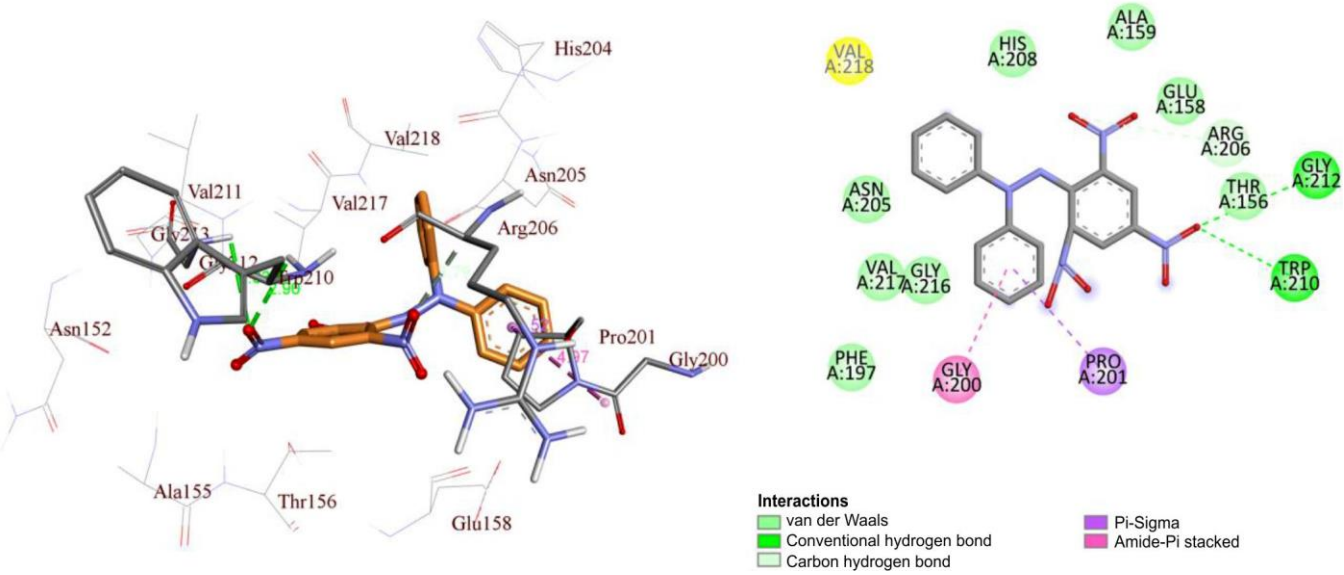

Fig. 6. 3D and 2D molecular docking outcome of DPPH

docking results matched the experimental biological activities well. *In vitro* activity was higher for compounds with superior binding affinity and interaction profile stability in the docking investigation, which explains their existence in biological activity. Molecules with lower docking scores (higher binding energy) exhibited stabilizing interactions such hydrogen bonding, hydrophobic contact and π-interactions, indicating more inhibitory potential. In contrast, molecules with lower *in silico* binding energies have lower experimental activity, proving that computational predictions match experimental data. In general, docking findings explain the activity pattern and support the structure-activity link found in experimental testing.

ADMET analysis: The *in silico* ADMET analysis was carried out for all the synthesised compounds **6a-l** in order to predict the physico-chemical and pharmacokinetic properties. Based on the obtain results (Table-2), the molecular weights (MW) of all compounds ranged from 318.15 to 396.06 g/mol, which fall within the acceptable limit (< 500 g/mol) stipulated by Lipinski's rule of five confirming their drug-like nature. This indicates that the molecular size of the compounds is favourable for passive diffusion and oral bioavailability. The topological polar surface area (TPSA) values were found to range from 52.30-95.44 $Å^2$, with most compounds (except **6a**, **6j** and **6l**) below the threshold of 90 $Å^2$ required for efficient BBB penetration. The relatively low TPSA values suggest good cell membrane permeability. The number of rotatable bonds was between 4 and 5, indicating moderate molecular flexibility suitable for favourable pharmacokinetic behaviour. All compounds exhibited five or fewer hydrogen bond acceptors (HBA) and no hydrogen bond donors (HBD = 0), suggesting minimal hydrogen bonding capacity another property conducive to enhanced lipophilicity and membrane permeability. The predicted log P values ranged from 4.006-5.873,

TABLE-2
ADMET ANALYSIS OF SYNTHESISED COMPOUNDS (**6a-l**)

Compound	MW	TPSA	NROTB	HBA	HBD	Log P	BBB	Lipinski's violation
6a	363.13	95.44	5	8	0	4.429	0.570	No
6b	352.11	52.30	4	5	0	5.323	0.689	No
6c	396.06	52.30	4	5	0	5.436	0.779	No
6d	386.07	52.30	4	5	0	5.860	0.733	No
6e	336.14	52.30	4	5	0	4.722	0.778	No
6f	318.15	52.30	4	5	0	4.637	0.839	No
6g	332.16	52.30	4	5	0	5.112	0.786	No
6h	360.16	69.37	5	6	0	4.006	0.599	No
6i	386.07	52.30	4	5	0	5.873	0.660	No
6j	363.13	95.44	5	8	0	4.530	0.631	No
6k	352.11	52.30	4	5	0	5.233	0.853	No
6l	363.13	95.44	5	8	0	4.384	0.693	No
Ascorbic acid	220.02	141.36	1	8	4	1.823	0.520	No

indicating moderate to high lipophilicity. The BBB permeability scores (0.57-0.85) further supported the potential of these compounds to cross the BBB effectively.

Conclusion

In this present work, a series of 12 new tetralone-fused triazole derivatives (**6a-l**) were synthesised and characterised them by ^{1}H NMR, ^{13}C NMR and LC-MS spectroscopic techniques. Further, all the compounds were assessed for their *in vitro* antioxidant properties by DPPH radical scavenging. The results demonstrate that compounds **6e**, **6h**, **6d** and **6i** possess significant radical-scavenging and membrane-protective activities. Among them, compound **6e** consistently exhibited the strongest activity across both DPPH and lipid peroxidation assays, with high inhibition percentages and low IC_{50} values, highlighting its superior ability to neutralize free radicals and prevent oxidative damage. The high relationship between DPPH scavenging and LPO inhibition also proves the effectiveness of these derivatives in inhibiting the initiation and propagation of oxidative stress. In general, compound **6e** has the potential to be the most promising antioxidant lead and it is worth developing it further in biological testing and potential use in the treatment of oxidative stress-related disease. Moreover, *in silico* molecular docking and ADMET analysis revealed protein ligand interaction with a reasonable docking energy and all the molecules displayed reasonable pharmacokinetic characteristics.

CONFLICT OF INTEREST

The authors declare that there is no conflict of interests regarding the publication of this article.

DECLARATION OF AI-ASSISTED TECHNOLOGIES

During the preparation of this manuscript, the authors used an AI-assisted tool(s) to improve the language. The authors reviewed and edited the content and take full responsibility for the published work.

REFERENCES

1. D. Hadjipavlou-Litina, I.E. Głowacka, J. Marco-Contelles and D.G. Piotrowska, *Antioxidants*, **12**, 36 (2023); https://doi.org/10.3390/antiox12010036
2. C.M. Mangione, M.J. Barry, W.K. Nicholson, M. Cabana, D. Chelmow, T.R. Coker, E.M. Davis, K.E. Donahue, C.A. Doubeni, C.R. Jaén, M. Kubik, L. Li, G. Ogedegbe, L. Pbert, J.M. Ruiz, J. Stevermer and J.B. Wong, *JAMA*, **327**, 2326 (2022); https://doi.org/10.1001/jama.2022.8970
3. K. Jomova, R. Raptova, S.Y. Alomar, S.H. Alwasel, E. Nepovimova, K. Kuca and M. Valko, *Arch. Toxicol.*, **97**, 2499 (2023); https://doi.org/10.1007/s00204-023-03562-9
4. M.H. Lin, C.F. Hung, H.C. Sung, S.C. Yang, H.P. Yu and J.Y. Fang, *Yao Wu Shi Pin Fen Xi*, **29**, 15 (2021); https://doi.org/10.38212/2224-6614.1151
5. A.B. Jena, R.R. Samal, N.K. Bhol and A.K. Duttaroy, *Biomed. Pharmacother.*, **162**, 114606 (2023); https://doi.org/10.1016/j.biopha.2023.114606
6. P. Chaudhary, P. Janmeda, A.O. Docea, B. Yeskaliyeva, A.F.A. Razis, B. Modu, D. Calina and J. Sharifi-Rad, *Front. Chem.*, **11**, 1158198 (2023); https://doi.org/10.3389/fchem.2023.1158198
7. Y. Hong, A. Boiti, D. Vallone and N.S. Foulkes, *Antioxidants*, **13**, 312 (2024); https://doi.org/10.3390/antiox13030312
8. B. Baccouri and I. Rajhi, In: *Terpenes and Terpenoids-Recent Advances*, IntechOpen (2021); https://doi.org/10.5772/intechopen.96638
9. E. Kabir and M. Uzzaman, *Results Chem.*, **4**, 100606 (2022); https://doi.org/10.1016/j.rechem.2022.100606
10. D.K. Slman, H.A. Satar, Z.A. Ketan and A.A. Jawad, *Al-Nahrain J. Sci.*, **27**, 19 (2024); https://doi.org/10.22401/ANJS.27.5.03
11. M.J. Nagesh Khadri, U. Shashikumar, P.-C. Tsai, K.B. Manjappa, V.K. Ponnusamy and S.A. Khanum, *ChemistrySelect*, **10**, e202403824 (2025); https://doi.org/10.1002/slct.202403824
12. N. Sivaraj, K. Sakthivel, K. Kikushima, M.D. Kostić, T. Dohi and F.V. Singh, *RSC Adv.*, **15**, 35509 (2025); https://doi.org/10.1039/D5RA06028A
13. J.J. Yang, W.W. Yu, L.L. Hu, W.J. Liu, X.H. Lin, W. Wang, Q. Zhang, P.-L. Wang, S.-W. Tang, X. Wang, M. Liu, W. Lu and H.-K. Zhang, *J. Med. Chem.*, **63**, 569 (2020); https://doi.org/10.1021/acs.jmedchem.9b01269
14. I.M. Bilai, V.I. Dariy, A.V. Khilkovets, A.I. Bilai and I.F. Duiun, *Curr. Issues Pharm. Med. Sci. Pract.*, **17**, 215 (2024); https://doi.org/10.14739/2409-2932.2024.3.311943
15. S. Kumar, S.L. Khokra and A. Yadav, *Future J. Pharm. Sci.*, **7**, 106 (2021); https://doi.org/10.1186/s43094-021-00241-3
16. S. Mohan, L. Krishnan, N. Madhusoodanan, A.D. Babysulochana, A. Sobha, N. Vankadari, J. Purushothaman and S.B. Somappa, *ACS Med. Chem. Lett.*, **15**, 1260 (2024); https://doi.org/10.1021/acsmedchemlett.4c00141
17. F.A.E. Fakayode, F.I. Imaghodor, A.O. Fajobi, B.O. Emma-Okon and O.O. Oyedapo, *J. Med. Pharm. Allied Sci.*, **10**, 3517 (2021); https://doi.org/10.22270/jmpas.V10I5.1511

18. D.B. Upadhyay, J.A. Mokariya, P.J. Patel, S.G. Patel, M.P. Parmar, D.P. Vala, F. Ferro, D.P. Rajani, M. Narayan, J. Kumar, S. Banerjee and H.M. Patel, *ACS Bio Med Chem Au*, **5**, 66 (2025); https://doi.org/10.1021/acsbiomedchemau.4c00060
19. J.A. Mokariya, A.G. Kalola, P. Prasad and M.P. Patel, *Mol. Divers.*, **26**, 963 (2022); https://doi.org/10.1007/s11030-021-10212-8
20. A. Garg, D. Borah, P. Trivedi, D. Gogoi, A.K. Chaliha, A.A. Ali, D. Chetia, V. Chaturvedi and D. Sarma, *ACS Omega*, **5**, 29830 (2020); https://doi.org/10.1021/acsomega.0c03862
21. H. Sung, J. Ferlay, R.L. Siegel, M. Laversanne, I. Soerjomataram, A. Jemal and F. Bray, *CA Cancer J. Clin.*, **71**, 209 (2021); https://doi.org/10.3322/caac.21660
22. A. Sharma, A.K. Agrahari, S. Rajkhowa and V.K. Tiwari, *Eur. J. Med. Chem.*, **238**, 114454 (2022); https://doi.org/10.1016/j.ejmech.2022.114454
23. N. Naeem, E.U. Mughal, A. Sadiq, G.A. Othman and B. Shakoor, *Arch. Pharm.*, **358**, 70059 (2025); https://doi.org/10.1002/ardp.70059
24. C. Tang, J. Liu, C. Yang, J. Ma, X. Chen, D. Liu, Y. Zhou, W. Zhou, Y. Lin and X. Yuan, *Biomolecules*, **12**, 1636 (2022); https://doi.org/10.3390/biom12111636
25. R.S. Patwardhan, D. Sharma and S.K. Sandur, *Transl. Oncol.*, **17**, 101341 (2022); https://doi.org/10.1016/j.tranon.2022.101341
26. T. Azim, M. Wasim, M.S. Akhtar and I. Akram, *BMC Complement. Med. Ther.*, **21**, 304 (2021); https://doi.org/10.1186/s12906-021-03485-x
27. B.A. Dar, A.R. Bhat, S. Ahmed, F.A. Sheikh, J. Jamalis, S.M.A. Kawsar, S.A. Sheikh, R.C. Patil and A. Abu-Rayyan, *In Silico Res. Biomed.*, **1**, 100094 (2025); https://doi.org/10.1016/j.insi.2025.100094
28. A. Jaggal, K.S. Katagi, M. Akki, V. Babagond, V. Kamat and S. Joshi, *J. Mol. Struct.*, **1320**, 139388 (2025); https://doi.org/10.1016/j.molstruc.2024.139388
29. M.N.S. Rad, S. Behrouz, F. Karimitabar and A. Khalafi-Nezhad, *Helv. Chim. Acta*, **95**, 491 (2012); https://doi.org/10.1002/hlca.201100324
30. M. Gutam, S. Mokenapelli, J.R. Yerrabelli, S. Banerjee, P. Roy and P.R. Chitneni, *Synth. Commun.*, **50**, 1883 (2020); https://doi.org/10.1080/00397911.2020.1759645
31. İ. Gulcin and S.H. Alwasel, *Processes*, **11**, 2248 (2023); https://doi.org/10.3390/pr11082248
32. S. Baliyan, R. Mukherjee, A. Priyadarshini, A. Vibhuti, A. Gupta, R.P. Pandey and C.-M. Chang, *Molecules*, **27**, 1326 (2022); https://doi.org/10.3390/molecules27041326
33. J. Xu, G. Guan, Z. Ye, C. Zhang, Y. Guo, Y. Ma, C. Lu, L. Lei, X.-B. Zhang and G. Song, *Sci. Bull.*, **69**, 636 (2024); https://doi.org/10.1016/j.scib.2023.12.036
34. A.C. Kumar, J. Rangaswamy, Madalambika, P.M. BharathKumar, P.R. Patil, M. Salavadi and N. Naik, *J. Mol. Struct.*, **1315**, 138749 (2024); https://doi.org/10.1016/j.molstruc.2024.138749
35. O. Trott and A.J. Olson, *J. Comput. Chem.*, **31**, 455 (2010); https://doi.org/10.1002/jcc.21334
36. S. Forli, R. Huey, M.E. Pique, M.F. Sanner, D.S. Goodsell and A.J. Olson, *Nat. Protoc.*, **11**, 905 (2016); https://doi.org/10.1038/nprot.2016.051
37. ADMETmesh, Online ADMET Prediction Tool, Available: https://admetmesh.scbdd.com/; Accessed on 29 August 2025.